AFRL-RV-PS-
TR-2021-0078

AFRL-RV-PS-
TR-2021-0078

REMOTE-EPITAXY OF MULTIJUNCTION SOLAR CELLS ON GRAPHENE COATED III-V SUBSTRATES

Jeehwan Kim

Massachusetts Institute of Technology
77 Massachusetts Avenue, Room NE18
Cambridge, MA 02139

26 Nov 2021

Final Report

APPROVED FOR PUBLIC RELEASE; DISTRIBUTION IS UNLIMITED.

See inside notice and signature page for additional restrictions.

AIR FORCE RESEARCH LABORATORY
Space Vehicles Directorate
3550 Aberdeen Ave SE
AIR FORCE MATERIEL COMMAND
KIRTLAND AIR FORCE BASE, NM 87117-5776

NOTICE AND SIGNATURE PAGE

Using Government drawings, specifications, or other data included in this document for any purpose other than Government procurement does not in any way obligate the U.S. Government. The fact that the Government formulated or supplied the drawings, specifications,or other data does not license the holder or any other person or corporation; or convey any rightsor permission to manufacture, use, or sell any patented invention that may relate to them.

This report is the result of contracted fundamental research which is exempt from public affairs security and policy review in accordance with AFI 61-201, paragraph 2.3.5.1. This report is available to the general public, including foreign nationals. Copies may be obtained from the Defense Technical Information Center (DTIC) (http://www.dtic.mil).

AFRL-RV-PS-TR-2021-0078 HAS BEEN REVIEWED AND IS APPROVED FOR PUBLICATION IN ACCORDANCE WITH ASSIGNED DISTRIBUTION STATEMENT.

//SIGNED//

DAVID WILT
Work Unit Manager

//SIGNED//

ANDREW SINCLAIR
Technical Advisor

//SIGNED//

JOHN BEAUCHEMIN
Chief Engineer

This report is published in the interest of scientific and technical information exchange, and its publication does not constitute the Government's approval or disapproval of its ideas or findings.

REPORT DOCUMENTATION PAGE

Form Approved
OMB No. 0704-0188

1. REPORT DATE *(DD-MM-YYYY)* 26-Nov-2021	**2. REPORT TYPE** Final Report	**3. DATES COVERED *(From - To)*** 26-Feb-2018 - 26-Nov-2021

4. TITLE AND SUBTITLE

Remote-Epitaxy Of Multijunction Solar Cells On Graphene Coated III-V Substrates

5a. CONTRACT NUMBER
FA9453-18-2-0017

5b. GRANT NUMBER

5c. PROGRAM ELEMENT NUMBER
62601F

6. AUTHOR(S)

Jeehwan Kim

5d. PROJECT NUMBER
8809

5e. TASK NUMBER
EF130439

5f. WORK UNIT NUMBER
V180

7. PERFORMING ORGANIZATION NAME(S) AND ADDRESS(ES)
Massachusetts Institute of Technology
77 Massachusetts Avenue, Room NE18
Cambridge, MA 02139

8. PERFORMING ORGANIZATION REPORT NUMBER

9. SPONSORING / MONITORING AGENCY NAME(S) AND ADDRESS(ES)
Air Force Research Laboratory
Space Vehicles Directorate
3550 Aberdeen Ave SE
Kirtland AFB, NM 87117-5776

10. SPONSOR/MONITOR'S ACRONYM(S)
AFRL/RVSV

11. SPONSOR/MONITOR'S REPORT NUMBER(S)
AFRL-RV-PS-TR-2021-0078

12. DISTRIBUTION / AVAILABILITY STATEMENT

Approved for public release, Distribution is unlimited.

13. SUPPLEMENTARY NOTES
Remote-Epitaxy Of Multijunction Solar Cells On Graphene Coated III-V Substrates

14. ABSTRACT

Lightweight, flexible, and highly efficient solar cells are desirable for high altitude and extraterrestrial photovoltaic (PV) applications to maximize the specific power. In this project, we have shown that graphene interlayer can be utilized as an effective technique to grow single-crystal thin films and solar cells that can be easily exfoliated precisely at the graphene interface. We have employed lateral overgrowth of GaAs on nanopatterned graphene-coated Ge substrates, as well as remote epitaxy of GaAs on graphene-coated III-V substrates, from which GaAs thin film is grown and exfoliated at the graphene interface. In both cases, graphene is directly grown on the substrate, which has enabled transfer defect-free large-scale formation of graphene. Single junction solar cells are successfully demonstrated by remote epitaxy on GaAs buffer.

15. SUBJECT TERMS
Remote epitaxy, III-V growth on graphene

16. SECURITY CLASSIFICATION OF:			**17. LIMITATION OF ABSTRACT**	**18. NUMBER OF PAGES**	**19a. NAME OF RESPONSIBLE PERSON**
a. REPORT	**b. ABSTRACT**	**c. THIS PAGE**			David Wilt
Unclassified	Unclassified	Unclassified	Unlimited	28	**19b. TELEPHONE NUMBER *(include area code)***

Standard Form 298 (Rev. 8-98)
Prescribed by ANSI Std. 239.18

--- This Page Intentionally Left Blank ---

TABLE OF CONTENTS

Page

LIST OF FIGURES

1. SUMMARY

Lightweight, flexible, and highly efficient solar cells are desirable for high altitude and extraterrestrial photovoltaic (PV) applications to maximize the specific power (W/kg). Currently, the heavy substrate is the limiting factor in maximizing the specific power, and to solve this issue, we aimed to utilize graphene as the interlayer to grow GaAs-based solar cells and exfoliate at the graphene interface to make light-weight and freestanding solar cells throughout this project. The motivation of this approach is based on the concept of remote epitaxy, which is recently invented by the PI, wherein semi-transparency of graphene allows single-crystalline thin films and devices to grow on graphene-coated substrates. Because of the weak van der Waals bonding between the graphene and the grown layer, the grown layer can be exfoliated precisely at the graphene interface by simple mechanical exfoliation, which provides a unique advantage to achieve fast, high yield, and post-release treatment-less exfoliation of epitaxially grown active layers for lightweight thin-film solar cell manufacturing. Although the preliminary study on remote epitaxy showed promise for making freestanding III-V devices, scaling up the process to make large-scale devices has been challenging.

Based on the preliminary results on remote epitaxy, we have investigated two different approaches to realize freestanding GaAs-based solar cells. The first approach is to employ nanopatterned graphene on Ge substrate. Because Ge has no ionicity and does not allow remote epitaxy to occur, we have patterned graphene on Ge substrate to locally expose the substrate for nucleation at the patterned region. GaAs is nucleated from the patterned region and laterally overgrown on graphene to form a fully merged single-crystalline GaAs film. Because most of the interface is still covered by graphene, exfoliation still occurs precisely at the graphene interface when the portion of exposed region is below a critical value. Since graphene is directly grown on Ge, this process is scalable and can be employed to make large-scale devices. We have also demonstrated that the substrate can be recycled without any refurbishing process to produce additional GaAs membranes by successive GaAs growth and peeling processes, since graphene mostly remains on the surface after peeling, substantiating the reusability of the substrate. The second approach is to utilize III-V surface for graphene formation. We have proposed to directly grow graphene on Ge wafer with a thin GaAs layer on top for solar cell growth, and to investigate the possibility of utilizing such III-V-on-Ge substrate for graphene growth, we started from GaAs wafers to grow graphene. We have found that bare GaAs surface is not stable at high temperature required for graphene growth, and thus we have developed graphene growth at a low temperature using a metal-organic chemical vapor deposition system with a toluene precursor. We used AlGaAs as a quasi-lattice-matched thermal buffer for graphene growth. By nanopatterning the graphene formed on AlGaAs/GaAs, GaAs thin film is grown that can be successfully exfoliated. In conclusion, throughout this project, we have shown that nanopatterned graphene interlayer can be utilized as an effective platform to grow single-crystal thin films that can be easily exfoliated precisely at the graphene interface. The film grown on nanopatterned graphene can be mechanically exfoliated at the graphene interface, and the substrate can be recycled to repeat the process. We envision that the proposed approach of utilizing 2D materials could not only be used for making freestanding solar cells, but has huge potential for 3D integration of dissimilar materials for high-performance and multi-functional devices.

2. INTRODUCTION

Lightweight, flexible, and highly efficient solar cells are desirable for high altitude and extraterrestrial photovoltaic (PV) applications to maximize the specific power (W/kg). Besides increasing the quantum efficiency, which is slowly nearing the theoretical limit, an alternative path to quickly increase the specific power is to reduce the weight of the solar arrays. Currently, the heavy substrate is the limiting factor in pushing the specific power beyond 1000 W/kg and, therefore, must be removed. Various methods have been developed over the decade for substrate removal, with chemical lift-off, optical lift-off, and laser lift-off being the dominant technology. However, even after a decade of development, the aforementioned methods have not been successful in securing adoption for mass production due to slow release rate of the active layers, low yield, and the need for post-release treatment of the host substrate [1].

In this project, we proposed to utilize the novel concept of remote epitaxy and graphene-based epitaxy and 2D material-based layer transfer (2DLT) technologies to achieve fast, high yield, and post-release treatment-less exfoliation of epitaxially grown active layers for lightweight thin-film solar cell manufacturing. The resulting thin-film multijunction solar cell will maintain high efficiency while being lightweight, flexible, and radiation hard due to the back surface metal allowing reduction of the base thickness by half. Remote epitaxy is a recently discovered method of epitaxy by the PI, Prof. Jeehwan Kim, where single-crystalline thin films are grown on graphene-coated substrates [2]. Because graphene is semi-transparent and does not completely screen the electrostatic surface fields fluctuation of the substrate, the material grown on top of graphene can be seeded by the substrate. Therefore, the epitaxial film grown on the graphene-coated substrate can follow the crystallinity of the substrate, as long as the ionicity of the substrate is high enough to ensure that the graphene does not fully screen the substrate [3]. The grown film can be exfoliated by depositing a metal stressor and by attaching a tape on top, followed by manual peeling from the sample edge. Because of the weak van der Waals bonding between graphene and the epilayer, exfoliation occurs precisely at the graphene interface, leaving an undamaged and pristine wafer behind. This exfoliation technique is termed as 2DLT by the PI, and various freestanding membranes including III-V, III-N, II-VI, and complex oxides are demonstrated so far by employing remote epitaxy and 2DLT [2, 3, 4]. Therefore, these methods provide an ideal technology to realize lightweight solar cells. Although the preliminary study on remote epitaxy showed promise for making freestanding III-V devices, scaling up the process to make large-scale devices has been challenging, mainly because graphene needs to be transferred onto the substrate of interest for III-V thin film growths. Also, remote epitaxy cannot be applied to elemental materials, such as Si and Ge, which hinders utilization of such low-cost elemental substrates to produce single-crystalline membranes and devices. Therefore, advanced methods to make the process more practical and scalable are necessary.

In this project, we aimed to expand the choice of substrate materials by employing nanopatterned graphene. One of the limitations of remote epitaxy is that the substrate material has to be ionic or partially ionic, so that the electrostatic potential fluctuation is strong enough and can penetrate through graphene. In other words, elemental materials like Ge do not have ionicity and remote epitaxy does not work for such materials. We have shown that elemental substrates such as germanium can work as a template for single-crystal thin film growth and exfoliation, when graphene interlayer is patterned. By nanopatterning graphene, we circumvented the limitation of remote epitaxy and realized GaAs thin film growth and exfoliation by selective seeding and lateral overgrowth. Antiphase boundaries were also effectively filtered out by employing nanopatterned graphene on on-axis Ge. We have also studied GaAs substrates coated by directly grown graphene for nanopattern-based approaches. Although GaAs can be grown on graphene-coated GaAs without patterning via remote epitaxy, preliminary results have shown that nanopatterning approach could improve the material quality of GaAs thin film grown on directly grown graphene, due to stronger bonding at the interface of patterned region. The capabilities to exfoliate grown nanomembranes and recycle the substrate using nanopatterned graphene suggest that the proposed approach could be an effective method to realize lightweight solar cells.

3. METHODS, ASSUMPTIONS, AND PROCEDURES

In this section, we describe the experimental methods and processes used throughout this project. Equipment used for the processes and experimental conditions are explained in detail. Step-by-step procedures to conduct experiments are also summarized.

3.1 Chemical vapor deposition (CVD) of graphene

Graphene is formed on Ge (100) wafers by a CVD growth process. We chose Ge as the substrate for GaAs thin film and solar cell growths because Ge is a low-cost substrate lattice-matched to GaAs. Although graphene is typically transferred onto inorganic semiconductor substrates due to the difficulties of direct growth on those substrates, we envisioned that direct growth is a better approach for large-scale device demonstration with high quality. This is because graphene transfer processes often induce defects, tearing, wrinkles, and residue. Also, the size of graphene is limited when transfer processes are employed.

Here, we used a CVD system shown in Figure 1 to grow graphene on Ge substrates. The CVD tube can be used for up to a 3-inch wafer, and thus CVD-grown graphene on Ge ensures wafer-scale or large-scale demonstration of thin film growth on graphene-coated Ge. The Ge wafer is first cleaned by diluted HCl (HCl : DI water = 1 : 3.5) for 2 minutes, followed by water rinsing and blow drying by nitrogen. Then, Ge substrate is loaded into the CVD tube, and the tube is purged for 30 minutes with Ar to flush residual air inside. Next, the temperature is increased up to 900-920°C by flowing 200 sccm of CH_4 and 730 sccm of H_2. Graphene is then grown at 900° C for 30 minutes with the same flow. After the growth, CH_4 and H_2 are shut off and the tube is cooled down with Ar flow of 140 sccm. The entire process is conducted at atmospheric pressure.

Figure 1. CVD system for graphene growth

3.2 Nanopattern based growth and exfoliation process

As mentioned in the introduction section, Ge is not an ionic material and thus remote epitaxy does not take place on graphene-coated Ge. Therefore, we envisioned that patterning the graphene to expose a periodic array of holes or lines will be a viable path for growth of single-crystalline thin films that can be exfoliated. The growth will first take place by nucleation at the patterned region where the graphene is etched away, followed by lateral overgrowth of the seed to form a merged film. As the growth continues, the film will be planarized and device structure such as solar cells can be grown on top of the planarized buffer, as shown in the schematic in Figure 2. After the growth, metal stressor and a tape can be deposited on the film to exfoliated film at the graphene interface.

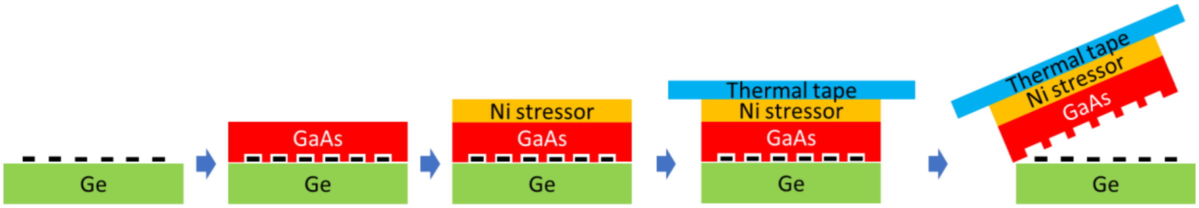

Figure 2. Graphene nanopattern-based process growth and exfoliation process

We have used electron beam lithography (EBL) and interference lithography to pattern graphene layers. EBL is used to study optimal geometry of nanopatterns to ensure high-quality GaAs growth and successful exfoliation. If the patterned region occupies too large portion, then exfoliation will fail because directly bonding at the patterned region, and thus the patterned region needs not be too large. On the other hand, if the portion of patterned region is made too small by increasing the pitch (periodicity) of the pattern, then the lateral overgrowth will not be sufficient to achieve merged and planarized thin films. Since EBL can precisely control the pattern geometry down to sub-10nm scale, we employed EBL to test various pattern geometries. We used a typical patterning process, starting with spin-coating e-beam resist on graphene-coated Ge samples. After e-beam writing, the resist is developed and then graphene is etched by reactive ion etching (RIE) using oxygen plasma. Lastly, the resist is cleaned by acetone and IPA rinsing. However, EBL process is not scalable and cannot be used for large-area patterning, which is necessary for making solar cells that are at least several-millimeter scales. Therefore, we have developed an interference lithography process to achieve large-area patterning. Interference lithography is a maskless lithography process that utilizes interference between two laser beams. When positive resist is used, only the region where the two beams constructively interfere is dosed sufficiently, and can be removed by developing. Line patterns can be made by a single exposure, and hole patterns can be made by a double exposure. As shown in Figure 3, we used a lift-off process to pattern large-area graphene by interference lithography. After exposure and developing, a 20 nm-thick SiO_2 is deposited by plasma-enhanced chemical vapor deposition (PECVD), followed by lift-off process by dipping the sample in acetone. Graphene is then etched by oxygen plasma etching, and SiO_2 mask is removed by dipping the sample in diluted HF and cleaning by DI water.

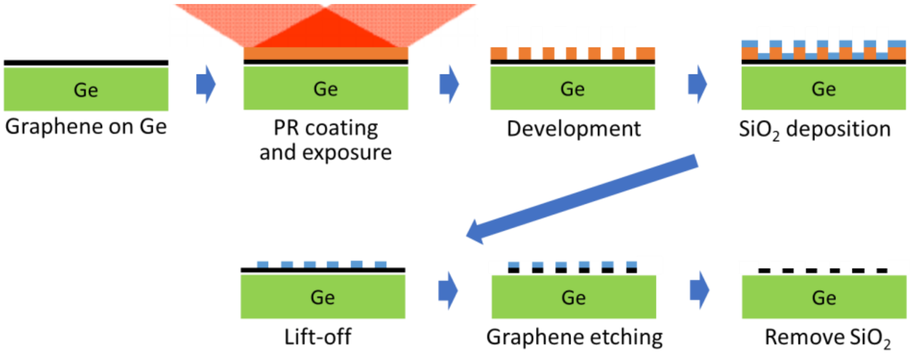

Figure 3. Interference lithography process to pattern graphene

Approved for public release, Distribution is unlimited.

3.3 Metal-organic chemical vapor deposition (MOCVD)

For epitaxial growth of GaAs thin films, we employed an MOCVD system, as shown in Figure 4. The MOCVD reactor is a vertical showerhead design, which can load six 2-inch wafers or one 6-inch wafer per growth. Nitrogen is used as a carrier gas, and trimethylgallium (TMGa) and arsine (AsH_3) are used for Ga and As precursors, respectively. GaAs growth on graphene-coated substrates was conducted by first ramping up the temperature to 650°C by flowing arsine to prevent substrate desorption. Next, GaAs is grown at 650°C with a V/III flow rate ratio of ~45 and a nominal growth rate of ~33nm/minute. After the growth, the reactor is cooled down to 300 °C under arsine overpressure.

Figure 4. MOCVD system for III-V and graphene growth

For solar cell growth and AlGaAs buffer growth, trimethylaluminum (TMAl), dimethylzinc (DMZn) and disilane (Si_2H_6) are used as sources of Al, Zn and Si, respectively, where Zn is used as a p-type dopant and Si is used as an n-type dopant. The detailed structure of GaAs solar cell is explained in the later section. The growth conditions of GaAs thin film and GaAs solar cell are kept the same regardless of the substrate, *i.e.* whether the substrate is a bare GaAs, a nanopatterned graphene-coated Ge, or graphene-coated III-V.

For graphene growth on III-V substrates, toluene is used as a carbon precursor. The reactor is ramped up to the graphene growth temperature, which is around 700-730°C, by flowing arsine, and then graphene is grown for 10-25 minutes by shutting off arsine and flowing toluene.

4.RESULTS AND DISCUSSION

4.1 CVD growth of graphene on Ge

CVD growth of graphene on Ge is highly sensitive to the growth temperature, because the melting point of Ge is relatively low, around 940°C. Because high-quality graphene is grown typically at 1,000°C or higher, which is higher than the melting temperature of Ge, it is typically desirable to grow graphene on Ge at the temperature very close to the melting point. Here, we optimized the graphene growth temperature at 900-920°C, which is right below the melting point. After the growth of graphene on Ge (100), the quality of the Ge surface and graphene is characterized.

First, the surface topography is characterized by atomic force microscopy (AFM), as shown in Figure 5(a). Under optimized growth conditions, the surface of graphene-coated Ge is extremely smooth with the roughness below 1 nm. This means that the Ge surface did not undergo melting or significant reconstruction of the surface. It is desirable to have smooth surface, because roughness could affect the patterning process and also the exfoliation process. Therefore, the roughness value below 1 nm is ideal for our study.

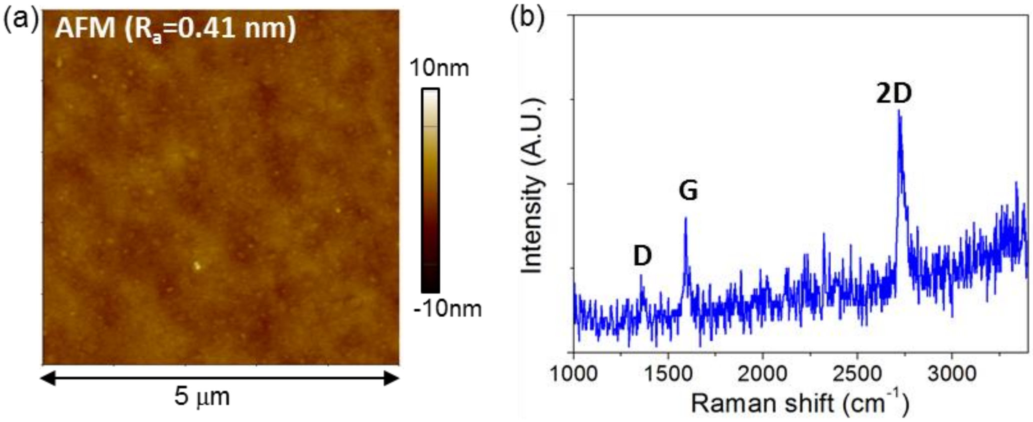

Figure 5. (a) AFM image and (b) Raman spectra of graphene grown on Ge

Next, the quality of graphene is characterized by Raman spectroscopy. As shown in Figure 5(b), the spectra exhibit signature graphene peaks, such as the D peak around 1,350 cm^{-1}, the G peak around 1,590 cm^{-1}, and the 2D peak around 2,690 cm^{-1}. The ratio between the intensity of 2D peak and G peak ((I(2D)/I(G)) is around two, wherein this high value represents that the average thickness of graphene is close to a monolayer. The D peak originates from defects in graphene, and since the D peak is significantly weaker than other peaks, the graphene quality is confirmed to be acceptable. Also, as graphene is used as a mask for lateral overgrowth, the electronic properties of graphene are not significantly important in this study. In other words, as long as the graphene layer is fully merged on Ge substrates without any damage on the substrate, the graphene could be utilized in studying selective growth of GaAs thin films and devices. Because the quality of graphene and the substrate confirmed by Raman spectra and AFM are satisfactory, the prepared graphene-coated Ge samples are used for patterning and growths.

4.2 Nanopatterning, epitaxy and exfoliation on graphene-coated Ge

As noted above, we have employed two different processes, electron-beam lithography and interference lithography, to investigate graphene nanopattern-based approaches. We have also studied two different patterns, 2D array of nanoholes and 1D array of lines, to study lateral overgrowth and exfoliation.

First, nanohole patterns of various dimensions are studied by electron-beam lithography. The SEM image in Figure 6 shows a representative pattern geometry after finishing the patterning process. Nanoholes with uniform sizes are periodically patterned by EBL, where the patterned region (the region where graphene is etched away and Ge is exposed) is shown as bright circles. Next, GaAs is grown on the nanopatterned graphene-coated Ge by MOCVD. After GaAs growth, the patterned region is clearly distinctive from the region where graphene is not patterned, as shown in Figure 7. Outside of the patterned region, multi-faceted polycrystalline film is observed, because GaAs randomly nucleated on graphene. On the other hand, planarized GaAs thin films are observed from the nanopatterned region. We observed a significant dependence between the periodicity of nanoholes and the planarization of GaAs. When the period is 350 nm and the hold diameter is 50 nm, the film is not fully planarized and faceted sidewalls are observed. On the other hand, when the period is decreased to 100 nm, the film is fully planarized, because merging of the film by lateral overgrowth occurred in earlier stage of the growth process. Therefore, to obtain fully planarized film without the need of very thick buffer, the distance between nanoholes needs to be small.

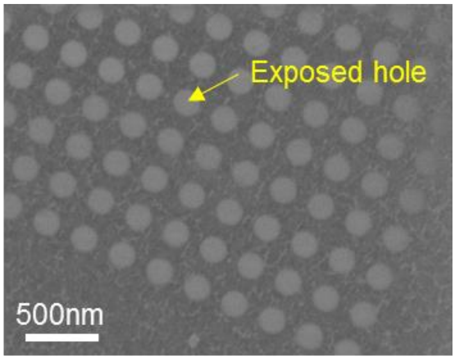

Figure 6. Nanohole array patterning on graphene by e-beam lithography

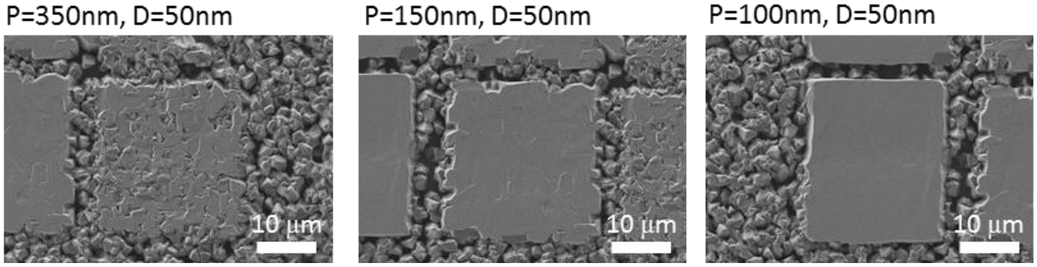

Figure 7. SEM images of GaAs grown on graphene nanohole arrays with different dimensions

Based on these findings, interference lithography is used to pattern the graphene over a larger area, so that larger GaAs film can be grown and be exfoliated. Step-by-step results are shown in the SEM images in Figure 8. After interference lithography and developing, periodic arrays of photoresist pillars are formed on the surface (Figure 8(a)). If periodic arrays of holes can be patterned instead of pillar, the next process of SiO_2 deposition for lift-off will not be necessary. However, controlling the dosage was more challenging to make hole patterns, and thus SiO_2 is deposited onto the sample, followed by acetone rinsing, which removes the photoresist pillars and SiO_2 atop. The SEM image in Figure 8(b) shows SiO_2 pattern on graphene-coated Ge. Using this SiO_2 mask, graphene of the unmasked region is etched by oxygen plasma treatment. Lastly, SiO_2 mask is removed by HF, and graphene nanohole patterns are formed on Ge, as shown in Figure 8(c), which is used as a template for large-area growth of GaAs. The periodicity of nanoholes is 400 nm, and the diameter of nanoholes is roughly 150 nm.

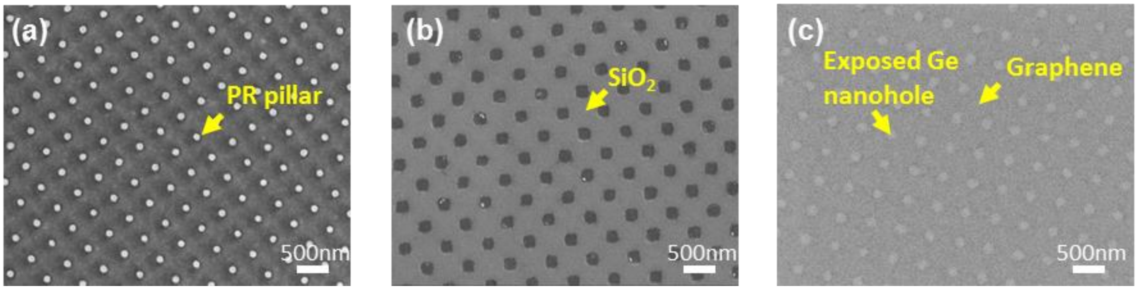

Figure 8. Interference lithography process. (a) After developing, (b) after SiO_2 lift-off, and (c) after completing the patterning

Next, GaAs is grown on the nanohole patterned graphene by MOCVD. The thickness of GaAs grown was nominally 3 μm, and after the growth, the film is mostly planarized, as shown in the SEM image in Figure 9(a). However, there was still some region that is not fully planarized. Electron backscattering diffraction (EBSD) image in Figure 9(b) reveals that the GaAs film formed on the graphene nanohole pattern (100) oriented single-crystalline.

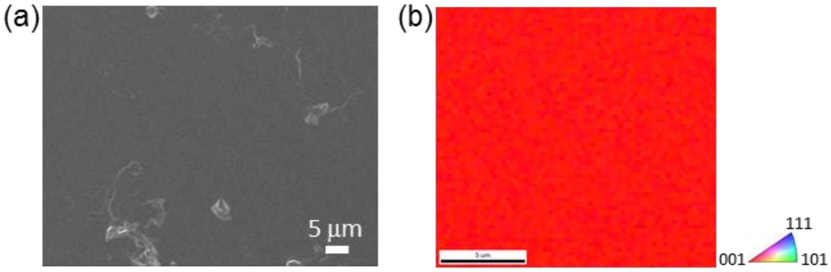

Figure 9. (a) SEM image of GaAs grown on nanopatterned graphene and (b) EBSD map

The grown GaAs film is exfoliated by depositing Ni as a stressor. First, a 30 nm-thick Ti layer is deposited by e-beam evaporation as an adhesion layer. Next, a few micrometer-thick Ni is sputtered on the sample. The Ni layer is tensile strained, and thus facilitates exfoliation of the film. A thermally releasable tape is attached on Ni, and the entire tape/Ni/GaAs stack is exfoliated mechanically from the sample edge. The photograph in Figure 10(a) shows perfectly exfoliated GaAs film (left) and the remaining Ge sample (right). Therefore, this result shows that the grown film can be exfoliated at the graphene interface, even with the presence of directly bonded region formed by nanopatterning process. The exfoliated Ge surface is further investigated by SEM measurements. As shown in the SEM images in Figure 10(b), the exfoliation occurred precisely at the graphene interface. Nevertheless, small stubs of GaAs is observed, rather than a completely smooth surface, because of the nanohole region where GaAs and Ge is directly bonded and fractured by the peeling process. In other words, although exfoliation was successful, the surface and the interface side of exfoliated film is not atomically smooth, and needs further processing if smooth surface is necessary.

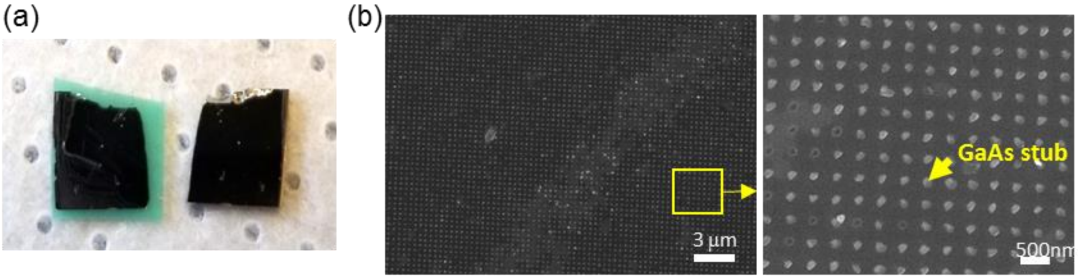

Figure 10. (a) Photograph of exfoliated film and substrate. (b) SEM images of exfoliated substrate

We note that graphene mostly remains on the substrate during the exfoliation process. Therefore, we have studied substrate reusability by directly regrowing GaAs thin film after exfoliation. Although nanopatterned regions exhibit GaAs stubs and slightly spalled features due to the random breakage of the film at the interface region without graphene, all those stubs are oriented along <001> direction. Therefore, he growth of GaAs on the exfoliated substrate was not affected by such roughened surface morphology, and the grown film showed single crystallinity. The GaAs film grown on the recycled substrate is successfully exfoliated, as shown in the photograph and SEM image in Figure 11(b). In the photograph, the dark color of Ge substrate after exfoliation means that the surface did not randomly spall, suggesting that exfoliation was successful throughout the entire sample region. Nevertheless, the size of the stubs and spalling on the exfoliated substrate slightly enlarged compared with the fresh sample (Figure 11(a) and (b)). We speculate that this is because graphene at the vicinity of the nanopatterned region is partially damaged during the exfoliation process, possibly due to the breakage of GaAs films at the directly bonded region. When the sample is recycled once more without any refurbishing process, the exfoliation was still successful for the entire sample region, although the damage on the substrate became more significant, as shown in the photograph and SEM images in Figure 11(c). This suggests that the graphene damage at the vicinity of the exposed region keeps occurring as the peeling process is repeated. After the fourth growth (third regrowth), exfoliation of the film was successful for only around 20 % of the sample region, as shown in the photograph in Figure 11(d). The gray region in the photograph is randomly spalled, and the size of stubs at the nanopatterned region of successfully exfoliated area became even larger, meaning that the graphene coverage was too low to ensure reliable exfoliation at the graphene interface. Therefore, these results show that the proposed nanopatterning approach allows substrate recycling without any refurbishing processes, although the graphene is partially damaged near the patterned region as the process is repeated. Therefore, if the pattern is made sufficiently small or the pitch is made large, it will be possible to recycle the substrate more than three times.

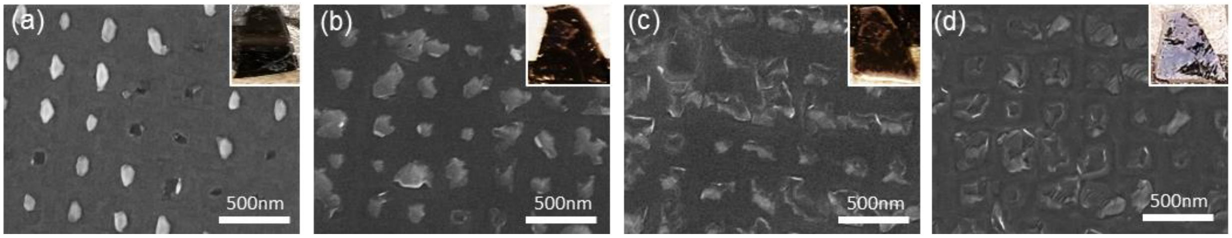

Figure 11. SEM images and photographs of Ge surface after exfoliating the grown film. (a) After first exfoliation, (b) after recycling the substrate once, (c) twice, and (d) three times

Although nanohole pattern-based approach yielded single-crystalline GaAs thin films that can be exfoliated, the grown film was not fully planarized even after growing 3 μm-thick GaAs on the nanohole patterns with the periodicity of 400 nm. Therefore, as an alternative design to more quickly planarize the surface, we have investigated line-shape patterns. As shown in the design in Figure 12(a), we have tried different periods, line widths, and rotation angles. The period represents the distance between each line patterns, and the width represents the width of each line pattern where the substrate is exposed, as shown in the SEM image in Figure 12(b). The rotation angle is the angle of the line with respect to the <110> direction, which is studied because lateral overgrowth rate is largely affected by the crystal direction and thus planarization will depend on the angle.

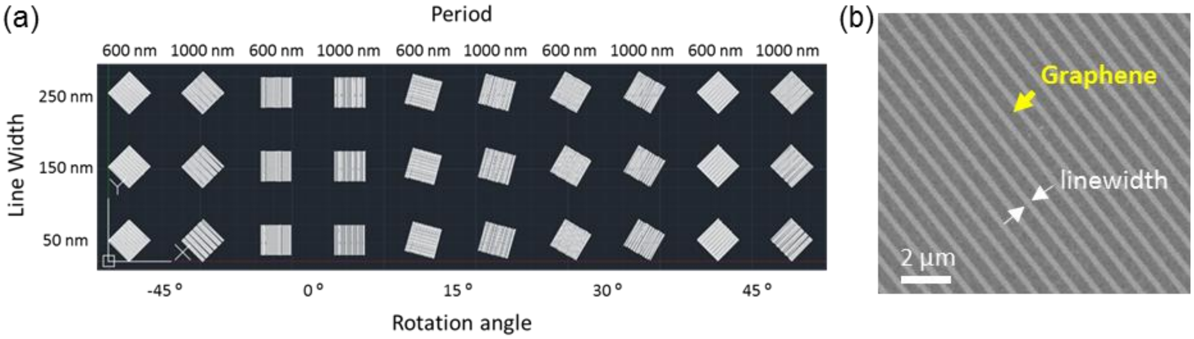

Figure 12. (a) Design of line patterns. (b) SEM image of line patterns on graphene

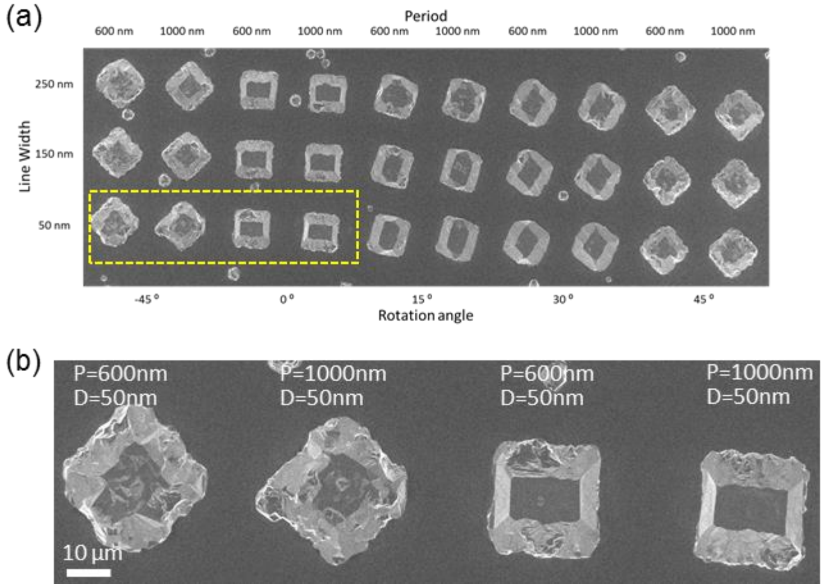

Figure 13. (a) SEM images of GaAs grown on nanopattern arrays with different geometry. (b) Zoom-in SEM of dashed region in (a)

This design is implemented by EBL process, followed by a growth of nominally 500 nm-thick GaAs film. As shown in Figure 13(a), GaAs formed merged films in all arrays, although the degree of planarization varied by the pattern geometry. Since slanted sidewalls are formed at the edge due to the finite size of the array, the morphology of the film in the center region (*i.e.* growth on top of the patterned region) is compared. In general, the growth from smaller pitch yielded slightly more planarized surface, while the opening width of the line did not significantly affect the morphology within the 50-150nm range. On the other hand, the orientation of the line patterns (rotation angle) significantly affected the morphology of the film. When the line pattern is oriented along <100> direction (45° and -45°), the film is very rough, as shown in Figure 13(b). The film morphology was better for other designs, meaning that the lateral overgrowth is suppressed when the line pattern is aligned to <100> direction. This information is utilized in doing large-area line patterning using interference lithography, which is described in the later section.

The GaAs film grown on EBL-patterned graphene-coated Ge is exfoliated by depositing Ni stressor and a thermally releasable tape, following the procedure described in the above section. Figure 14(a) shows the SEM image of Ge surface after the exfoliation. The exfoliation yield is color-coded. As expected, the pattern geometry with larger graphene coverage (smaller diameter and larger period) showed better exfoliation. On the other hand, if the exposed area occupies larger portion, the entire GaAs film is not successfully exfoliated, but randomly spalled. This is because the directly bonded portion between GaAs and Ge makes strong bonding at the interface. When the period was 1,000 nm, exfoliation was mostly successful for the entire range of line widths. On the other hand, at 600 nm period, exfoliation was successful only for the case of and the orientation of line patterns. When the exfoliation of GaAs film was successful, line-shape damage is left behind on the surface, which corresponds to the patterned region, as shown in Figure 14(b). Here, we note that the planarization of GaAs film was much more effective when line-shaped pattern is employed, compared with the case of hole patterns. Since the GaAs film can still be exfoliated by lateral overgrowth from line patterns, we conclude that using a line-shaped pattern is a better approach for growing GaAs film and exfoliating.

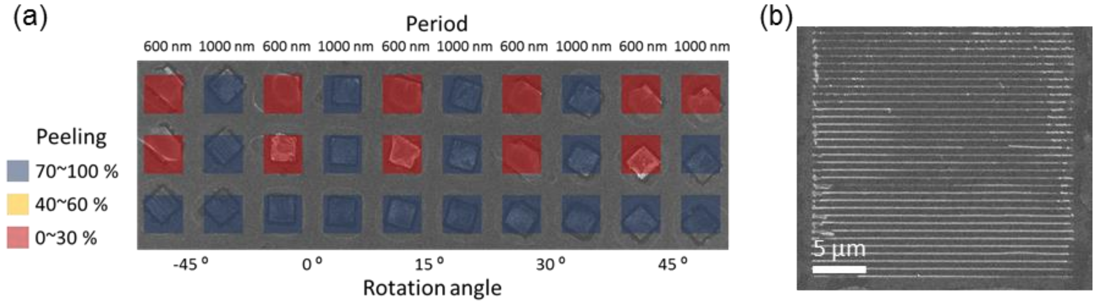

Figure 14. (a) SEM image of exfoliated surface with color-coded exfoliation yield. (b) SEM image of successfully exfoliated region

Based on the results obtained from EBL patterning, large-area graphene line patterns are prepared by interference lithography. As noted above, line patterning requires only one cycle of exposure to generate the interference pattern, and thus it is easier to control the dimension. Since 1,000 nm pitch showed both well-planarized GaAs film and perfect exfoliation, large-area pattern with the same 1,000 nm pitch is prepared by interference lithography. The prepared graphene pattern is shown in Figure 15(a), which shows uniform line-shaped pattern with a pitch of 1,000 nm and a width of around 350 nm. Next, a nominally 2 µm-thick GaAs film is grown on the line-patterned graphene-coated Ge. As shown in the SEM image in Figure 15(b), the film is completely planarized after the growth, meaning that lateral overgrowth is significantly faster on line pattern compared with the case of hole pattern with the same periodicity. We also note that the film grown on nanopatterned graphene-coated Ge is free of antiphase boundaries (APBs), whereas GaAs directly grown on Ge shows high density of APBs, as shown in the SEM image in Figure 15(c). Since the formation of APBs on on-axis group IV materials difficult to eliminate or mitigate, APB-free GaAs film formed on on-axis Ge by employing nanopatterned graphene could significantly improve the material quality and device quality of GaAs devices grown on Ge.

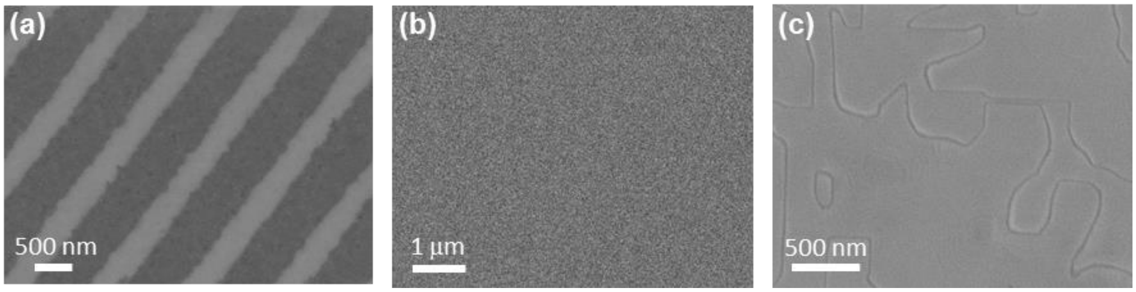

Figure 15. SEM images of (a) graphene patterned by interference lithography and (b) after GaAs growth. (c) GaAs directly grown on Ge wafer

After growth of GaAs thin film on interference lithography-patterned graphene, the sample is exfoliated by depositing a Ni stressor and attaching a thermally releasable tape. The exfoliation was successfully conducted, even though the line width formed by interference lithography (350 nm) is wider than the dimension used in EBL study. The exfoliation occurred precisely at the graphene interface as shown in Figure 16(a), with a spalling at the patterned region which is more clearly shown in the SEM image in Figure 16(b). Therefore, these results suggest that nanopatterned graphene on Ge can be employed as a template for the growth of GaAs thin films and devices which can be exfoliated at the graphene interface. We compared hole and line patterns, and line patterns showed clear advantage in quickly planarizing the GaAs buffer by faster lateral overgrowth. Therefore, by growing GaAs solar cell structure on top of the GaAs buffer, the solar cell layer can be exfoliated to make it freestanding and lightweight.

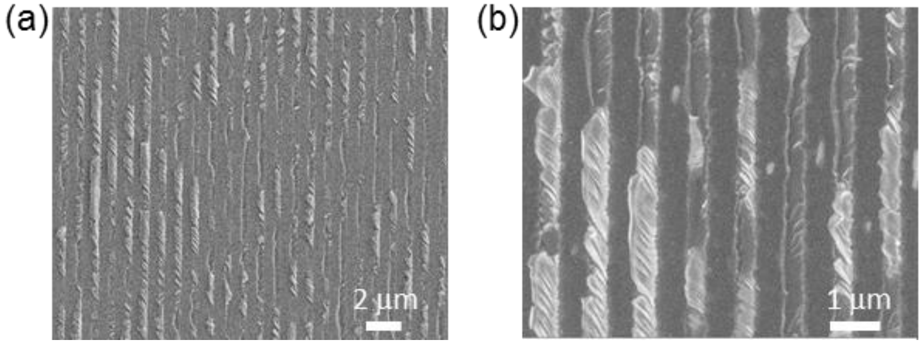

Figure 16. SEM images of substrate after exfoliation

4.3 Graphene growth on III-V and GaAs growth

Unlike Ge, III-V compound semiconductors such as GaAs, InP and InAs are partially ionic and remote epitaxy can occur through a monolayer graphene. Therefore, patterns are not necessary for growing single-crystal III-V films on graphene-coated III-V substrates. Although remote epitaxy of III-V thin films has been experimentally demonstrated by transferring graphene onto III-V [2], it is critical that the graphene has to be monolayer and the interface has to be pristine without any transfer residue or native oxides for successful remote epitaxy [3, 5]. Since this requirement is hard to satisfy over large area when transferred graphene is used, it is challenging to demonstrate large-scale devices by remote epitaxy of III-V when transferred graphene is employed. Also, even in the case of nanopatterning approach, the same issues need to be resolved for scalable and residue-free thin film growths. Therefore, we have attempted to directly grow graphene on III-V. If this is made feasible, graphene formed on III-V will be transfer defect-free and can be easily made in wafer-scale.

One of the challenges in directly growing graphene on III-V is that III-V surface is typically not stable at the graphene growth temperature, which is >1,000°C for typical graphene growth and 900-920°C for growth in Ge. Also, the cracking efficiency of methane drops quickly below 900°C, which makes low-temperature growth of graphene difficult. To circumvent these, we adopted toluene (C_7H_8) as a carbon source that cracks at much lower temperature, with effective cracking even at below 600°C under the graphene growth environment. The toluene precursor is installed to our III-V MOCVD system, which provides a possibility of growing graphene and III-V layer in a single growth run.

The growth of graphene on GaAs by toluene precursors was studied over a wide range of growth conditions, but the GaAs surface degraded before the graphene formation at relatively high temperatures, and graphene did not form at lower temperatures. We therefore grew AlGaAs layer first, which is quasi-lattice matched to GaAs, as a thermal buffer for graphene growth, as shown in the process schematic in Figure 17. Since AlGaAs is thermally more robust at high temperature, we were able to successfully grow graphene on the AlGaAs layer. The ideal graphene temperature is found to be around 700-730°C. After the graphene growth, GaAs thin film or solar cell layer is grown and exfoliated. We have investigated both nanopatterned and non-patterned graphene on AlGaAs/GaAs for growth of GaAs.

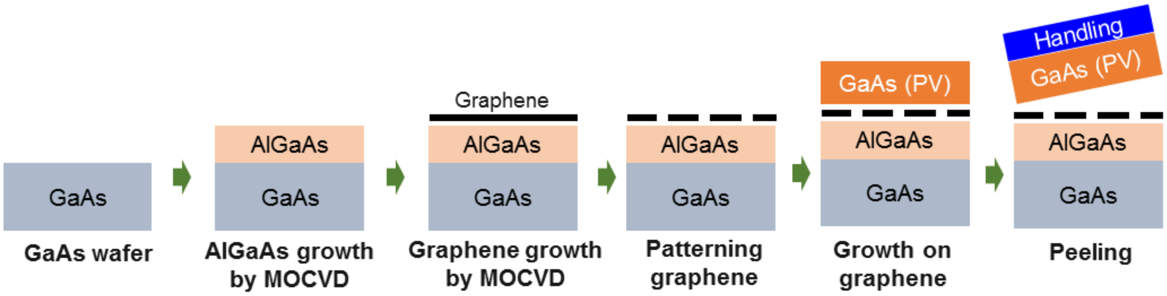

Figure 17. Process flow of remote epitaxy and 2DLT using directly grown graphene

The properties of directly grown graphene on AlGaAs/GaAs are shown in Figure 18. The surface of graphene-grown AlGaAs remains atomically smooth with the roughness of 0.19 nm. This means that the substrate was not damaged at the growth temperature of graphene. The Raman spectra in Figure 18(b) show the D, G, 2D peaks at around 1,350 cm^{-1}, 1,590 cm^{-1}, and 2,900 cm^{-1}, respectively. Unlike the case of graphene grown on Ge, all three peaks showed significant broadening. This is because the graphene growth temperature is much lower than the ideal graphene growth temperature. Because of the low growth temperature, graphene did not form a well-ordered single-crystalline hexagonal structure, but rather formed an amorphous-phase graphene. The Raman spectra agree perfectly with the amorphous monolayer graphene reported by another group [6], suggesting that the graphene formed on AlGaAs is monolayer but in an amorphous phase. Because graphene's electronic properties are not critically important in our approach as graphene is not a part of the device, we anticipate that the phase of graphene will not significantly affect the remote epitaxy property as long as the thickness of graphene is thin enough. Also, if the graphene is patterned for growth, the thickness of graphene also may not critically matter, as lateral overgrowth will be the dominant growth mechanism.

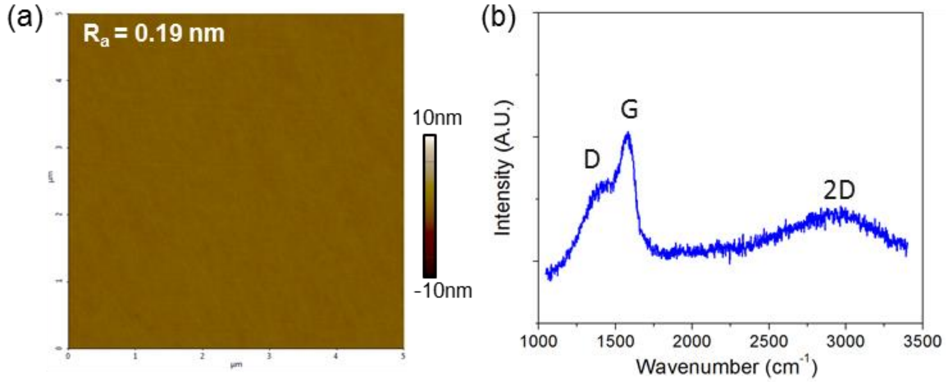

Figure 18. (a) AFM image and (b) Raman spectra of directly grown graphene

Next, amorphous graphene is patterned, following the same process as Ge nanopattern formation, which is described above in detail. Figure 20(a) shows the SEM image of line-patterned graphene on AlGaAs/GaAs substrate by e-beam lithography. A 500 nm-thick GaAs film is grown on the nanopatterned graphene-coated AlGaAs/GaAs substrate at 650°C, and the results are compared with the case of remote epitaxy. The GaAs thin film formed on nanopatterned graphene (Figure 19(b)) has shown more planarized surface with lower density of line-defects when compared with the case of remote epitaxy (Figure 19(d)), wherein 500 nm-thick GaAs is grown on the same graphene/AlGaAs/GaAs template but without patterning. This means that the thickness of the GaAs films was not high enough to fully planarize the films for both cases. For the case of patterned graphene, the planarization is affected by the lateral overgrowth and thus could be enhanced by optimizing the pattern geometry and growth condition to promote lateral overgrowth. For the case of remote epitaxy (*i.e.* without pattern), the rough morphology originates from islands growth mode on graphene, not layer-by-layer growth mode, due to the low surface energy of graphene, and thus the film could be more quickly smoothened by optimizing the nucleation condition to make higher density of nuclei on graphene in the nucleation stage. It should also be noted that there could be a mixed-growth mode between lateral overgrowth from patterned region and remote nucleation on graphene region in the formal case, affecting the overall material quality of the merged film. Because the exposed region provides a site for strong covalent bonding, nanopatterning the graphene layer could enable improved material quality, and the quality could be affected by the thickness of graphene which will change the portion of remote epitaxy to lateral overgrowth. The GaAs film grown on nanopatterned graphene is successfully exfoliated, as shown in the SEM image in Figure 19(c), substantiating the feasibility of utilizing nanopatterned graphene on AlGaAs/GaAs for freestanding membrane production.

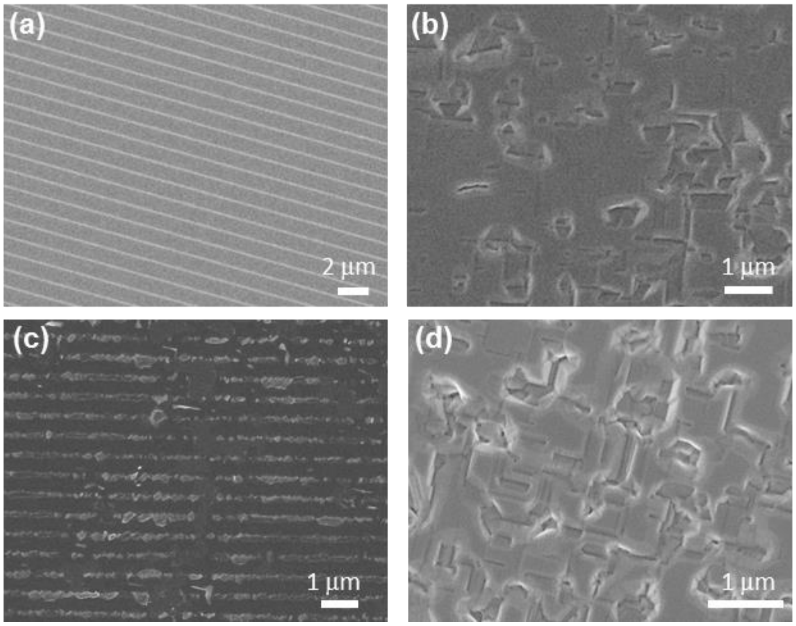

Figure 19. (a) SEM images of nanopatterned graphene on AlGaAs/GaAs substrate, (b) after GaAs growth, and (c) after exfoliation of the grown film. (d) SEM image of GaAs grown directly on non-patterned graphene

Although we have not demonstrated solar cell structures on nanopatterned graphene samples, we have grown and characterized GaAs solar cells grown by remote epitaxy, as a part of a separate project funded by Depart of Energy – Solar Energy Technologies Office (DE-EE0008558). The structure of the solar cell is schematically shown in Figure 20(a). The fabricated cells are characterized under the standard AM 1.5 condition, and the photoconversion efficiency (PCE) is measured from the I-V curve in Figure 20(b). The remote epitaxial solar cell on grown graphene (blue line) exhibited a PCE of 7.9%. The control cell which is directly grown on GaAs wafer showed a PCE of 9.1%. Since we did not deposit an anti-reflection coating layer, the PCE is not very high even for the cell grown on a bare GaAs wafer. Also, the doping of the structure may not be well-controlled. Smaller PCE and decreased external quantum efficiency (EQE) at long-wavelength regime (Figure 20(c)) indicate that the photons absorbed at the lower region of the cell did not contribute to the photocurrent as efficiently, implying that there will be higher density of crystal defects in the cells grown by remote epitaxy. We speculate that the higher defect density in the cells grown by remote epitaxy in the DOE project (DE-EE0008558) is due to the nucleation mode as discussed above, and therefore could be improved by optimizing the nucleation condition of GaAs buffer on graphene. Also, since nanopattern-based approach can provide direct nucleation sites for improved crystal quality compared with the case of remote epitaxy, we envision that nanopatterning graphene could yield higher efficiency solar cells than remote epitaxy, which will be investigated as future work.

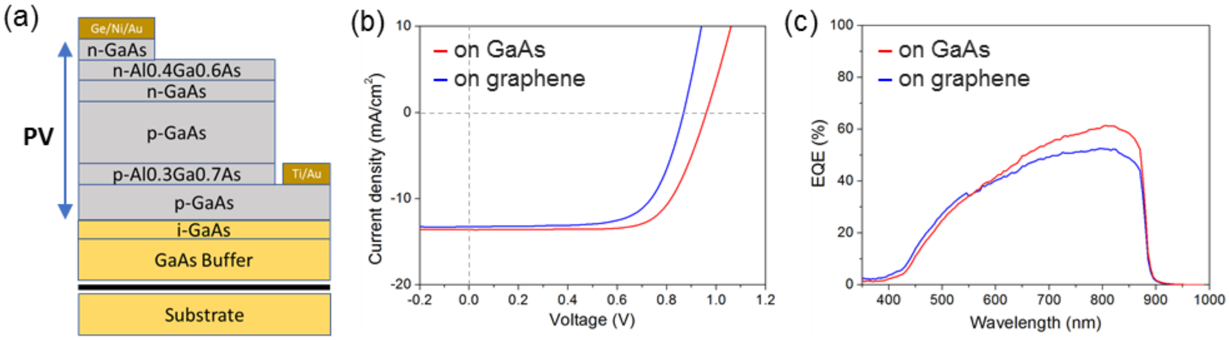

Figure 20. (a) Remote epitaxy solar cell structure. (b) I-V curve of solar cells under 1.5 AM and 1 Sun. (c) EQE as a function of wavelength. All data are adapted from DOE project (DE-EE0008558)

5. CONCLUSIONS

In this project, we have investigated two different substrates to realize freestanding GaAs-based solar cells that are lightweight and detached from the wafer. First, graphene is directly grown on Ge substrate, followed by nanopatterning to locally expose the substrate, because remote epitaxy does not work on elemental substrates. The patterned region works as a nucleation site of GaAs, and then GaAs is laterally overgrown to form a fully merged thin film. With the optimized geometry, well-planarized and APB-free GaAs thin film is grown by this approach, and exfoliated successfully at the graphene interface. The substrate could be recycled several times without any refurbishing process. In the second approach, graphene is directly grown on III-V substrates by developing a low-temperature graphene growth process to prevent damage of III-V substrates, from which amorphous phase graphene is formed on III-V surface. Nanopatterning the graphene has resulted in improved material quality of GaAs film compared with remote epitaxy on non-patterned graphene.

As future work, we envision that improving the material quality of GaAs buffer on graphene is the key to make the PCE as good as the control cell, for both Ge and AlGaAs/GaAs substrates. The lateral overgrowth condition can be further optimized by tuning the growth condition to maximize the rate of lateral to vertical growth, which will ensure quick planarization of GaAs film grown from nanopatterned graphene. By this, the periodicity of nanopatterns can be made much larger, which will ensure recycling of the substrate more than a few times, since the surface will still be mostly covered by graphene after repeated growth and exfoliation processes. Unlike the case of graphene-coated Ge where the growth is purely driven by selective area epitaxy followed by lateral overgrowth, mixed growth modes could exist in graphene-coated AlGaAs/GaAs substrates, and thus the effect of the thickness of graphene on AlGaAs/GaAs will be studied for GaAs film quality. Since the surface of the exfoliated film (interface side) is not flat due to the spalling at the nanopatterned region, it will be necessary to develop an etching process to planarize the surface after peeling, or alternatively, utilizing the nanostructure for anti-reflection could be studied. Because nanopatterned graphene can be universally utilized for the production of freestanding membranes including elemental substrates, further development of graphene nanopattern-based epitaxy will enable heterointegration of various materials to realize new functionalities.

REFERENCES

[1] H. Kum, D. Lee, W. Kong, H. Kim, Y. Park, Y. Kim, Y. Baek, S.-H. Bae, K. Lee, and J. Kim, “Epitaxial growth and layer-transfer techniques for heterogeneous integration of materials for electronic and photonic devices”, *Nature Electronics*, **Vol. 2**, pp. 439-450, 2019.

[2] Y. Kim, S. S. Cruz, K. Lee, B. O. Alawode, C. Choi, Y. Song, J. M. Johnson, C. Heidelberger, W. Kong, S. Choi, K. Qiao, I. Almansouri, E. A. Fitzgerald, J. Kong, A. M. Kolpak, J. Hwang, and J. Kim, “Remote epitaxy through graphene enables two-dimensional material-based layer transfer”, *Nature*, **Vol. 544**, pp. 340-343, 2017.

[3] W. Kong, H. Li, K. Qiao, Y. Kim, K. Lee, Y. Nie, D. Lee, T. Osadchy, R. J. Molnar, D. K. Gaskill, R. L. Myers-Ward, K. M. Daniels, Y. Zhang, S. Sundram, Y. Yu, S.-H. Bae, S. Rajan, Y. Shao-Horn, K. Cho, A. Ougazzaden, J. C. Grossman and J. Kim, “Polarity governs atomic interaction through two-dimensional materials” *Nature Materials*, **Vol. 17**, pp. 999-1004, 2018.

[4] H. S. Kum, H. Lee, S. Kim, S. Lindemann, W. Kong, K. Qiao, P. Chen, J. Irwin, J. H. Lee, S. Xie, S. Subramanian, J. Shim, S.-H. Bae, C. Choi, L. Ranno, S. Seo, S. Lee, J. Bauer, H. Li, K. Lee, J. A. Robinson, C. A. Ross, D. G. Schlom, M. S. Rzchowski, C.-B. Eom, and J. Kim, “Heterogeneous integration of single-crystalline complex-oxide membranes”, *Nature*, **Vol. 578**, pp. 75-81, 2020.

[5] H. Kim, K. Lu, Y. Liu, H. S. Kum, K. S. Kim, K. Qiao, S.-H. Bae, S. Lee, Y. J. Ji, K. H. Kim, H. Paik, S. Xie, H. Shin, C. Choi, J. H. Lee, C. Dong, J. A. Robinson, J.-H. Lee, J.-H. Ahn, G. Y. Yeom, D. G. Schlom, and J. Kim, “Impact of 2D−3D Heterointerface on Remote Epitaxial Interaction through Graphene”, ACS Nano, **Vol. 15**, pp. 10587-10596, 2021.

[6] C.-T. Toh, H. Zhang, J. Lin, A. S. Mayorov, Y.-P. Wang, C. M. Orofeo, D. B. Ferry, H. Andersen, N. Kakenov, Z. Guo, I. H. Abidi, H. Sims, K. Suenaga, S. T. Pantelides, and B. Ozyilmaz, “Synthesis and properties of free-standing monolayer amorphous carbon”, *Nature*, **Vol. 577**, pp. 199-203, 2020.

LIST OF ACRONYMS, ABBREVIATIONS, AND SYMBOLS

Acronym/ Abbreviation	**Description**
2DLT	2D material-based layer transfer
CVD	Chemical vapor deposition
MOCVD	Metal-organic chemical vapor deposition
EBL	Electron beam lithography
SEM	Scanning electron microscopy
AFM	Atomic force microscopy

Symbol	**Description**
R_a	Average roughness

DISTRIBUTION LIST

DTIC/OCP 8725 John J. Kingman Rd, Suite 0944 Ft Belvoir, VA 22060-6218	1 cy
AFRL/RVIL Kirtland AFB, NM 87117-5776	1 cy
Official Record Copy AFRL/RVS/David Wilt	1 cy